Journal of Optics

PAPER

A method of depth extension in 3D shape measurement by geometric constraints

IOP Publishing Journal of Optics
J. Opt. **22** (2020) 125701 (8pp) https://doi.org/10.1088/2040-8986/abc089

A method of depth extension in 3D shape measurement by geometric constraints

Shenzhen Lv[1,2], Yuyuan Zhang[3], Jian Wang[1] and Qiang Sun[1]

[1] R&D Center of Precision Instruments and Equipment, Changchun Institute of Optics, Fine Mechanics and Physics, Chinese Academy of Sciences, No.3888, Dongnanhu Road, Changchun, Jilin, People's Republic of China
[2] University of Chinese Academy of Sciences, Beijing 100049, People's Republic of China
[3] College of Science, Jilin Institute of Chemical Technology, Jilin 132022, People's Republic of China

E-mail: sunq@ciomp.ac.cn

Received 11 July 2020, revised 16 September 2020
Accepted for publication 13 October 2020
Published 29 October 2020

Abstract

In this paper a new method to extend the measurement depth limited by geometric constraints for objects with large depth variances is presented. This method mainly includes the following steps: (1) using the watershed image segmentation algorithm to extract the correct part of the discontinuous absolute phase distribution obtained by geometric constraints, and making a binary mask of the correspondent region; (2) using the window Fourier filter-quality guided phase unwrapping algorithm to obtain the relative phase distribution of the tested object; (3) using the binary mask to get the difference between the relative and the absolute phases; (4) converting the relative phase distribution to absolute phase distribution by referring to their phase difference in the mask region. The experimental results prove the effectiveness and correctness of the proposed method.

Keywords: optical metrology, geometric constraints, fringe analysis, absolute phase

(Some figures may appear in colour only in the online journal)

1. Introduction

As one of the most popular techniques for non-contact three-dimensional (3D) measurement, fringe projection profilometry has been growing rapidly and has been applied in diverse fields [1–4]. In this technique the phase recovery from the fringe patterns is required and there exist many methods for this task [5–8]. Generally, the above fringe analysis methods only produce a wrapped phase map with 2π discontinuities. To obtain a continuous phase map, the wrapped phase needs to be unwrapped including the temporal phase unwrapping (TPU) [9, 10] and the spatial phase unwrapping (SPU) [11].

In recent years, An *et al* [12] proposed a geometric constraints-based absolute phase unwrapping method that had merits of robustness to noise, high-speed and high-accuracy. Compared with TPU, geometric constraint method only uses the internal and external parameters of the system without requiring additional image acquisition, which can effectively improve the speed and quality of the 3D measurement. As compared with SPU, absolute 3D geometry information of tested objects can be acquired and multiple separate objects can be simultaneously measured by this method. Since no additional image acquisition is required, the geometric constraint method can be effectively used for the measurement of high-speed moving objects [13]. Based on [12], we presented a monotonic discriminant to determine the correct position of the virtual plane in geometric constraint method for different cases [14]. In addition, the geometric constraint method has also been applied to other phase recovery methods to improve the accuracy and speed of 3D measurement [15–17].

However, as mentioned by An *et al* [12] the geometric constraint method is limited to the measurement of a certain depth range, making it difficult to measure objects with large depth variances or objects moving in a large depth range. Dai *et al*

[18] proposed a method using a known object (i.e. a ping-pong ball) to provide dynamic virtual plane positions to achieve the measurement of objects moving along depth direction. Duan *et al* [19] proposed an adaptive method to extend the motion range of objects. For the measurement of objects with large depth variances, Jiang *et al* [20] proposed a method combining multiple different unwrapped phase maps created with multiple different virtual planes to extend the measurement depth range.

In Jiang's method, firstly the closest distance plane, $z^w = z_{\min}$, is selected as first virtual plane to generate an absolute phase map of $\Phi^1_{\min}$. The correspondent unwrapped phase map of Φ^1 is with the effective depth from $z_{\min}$ to $z_{\max}$, giving a measurement depth range of Δz. Then the distance, $z^w = z_{\max}$, is selected as second virtual plane to generate a new absolute phase map of $\Phi^2_{\min}$. The correspondent unwrapped phase map of Φ^2 is with the effective depth from $z_{\max}$ to $z_{\max} + \Delta z$. Properly combining Φ^1 and Φ^2, the effective measurement depth range can be extended to $2\Delta z$. Obviously, as the number of virtual planes increases continuously, the effective measurement depth range of the phase unwrapping increases correspondently. However, as described in [20], the larger the depth range of the object to be measured, the more virtual planes are required. This means that more feature points' extraction and more complex algorithm of the region segmentation are required.

In this paper, we present a new method based on windowed Fourier-filtered and quality-guided phase-unwrapping algorithm [21] (WFF-QGPU) to extend the measurement depth range of the geometric constraint method for objects with large depth variances. This method possesses the following two advantages: (i) window Fourier transform (WFT) is a redundant transform, and its spectrum reflects the local characteristics of a signal. Thereby, the noise in the wrapped phase map can be well suppressed. (ii) The region segmentation process is simple which we only need to select a virtual plane and extract correspondent effective interval of absolute phase unwrapping. The experimental measurement results of two different objects with large depth variances prove the effectiveness of the proposed method.

The structure of this paper is as follows. Section 2 explains the principle of the proposed method; section 3 shows the experimental results; section 4 discusses the merits and limitation of the proposed method; section 5 summarizes the article.

2. Principles

2.1. Three-step phase shifting algorithm

Mathematically, the fringe patterns of three-step shift algorithm can be expressed as:

$$I_1(x,y) = I'(x,y) + I''(x,y)\cos\left(\Phi(x,y) - \frac{2\pi}{3}\right), \quad (1)$$

$$I_2(x,y) = I'(x,y) + I''(x,y)\cos(\Phi(x,y)), \quad (2)$$

$$I_3(x,y) = I'(x,y) + I''(x,y)\cos\left(\Phi(x,y) + \frac{2\pi}{3}\right), \quad (3)$$

where $I'(x,y)$ and $I''(x,y)$ are the average intensity and intensity modulation, respectively, and $\Phi(x,y)$ is the phase to be retrieved. Solving equations (1)-(3) leads to

$$\phi_w(x,y) = \tan^{-1}\left[\frac{\sqrt{3}(I_1 - I_3)}{2I_2 - I_1 - I_3}\right], \quad (4)$$

where ϕ_w is the wrapped phase ranging from $-\pi$ to π. In order to obtain a continuous phase map, the wrapped phase needs to be unwrapped, which is expressed as:

$$\Phi(x,y) = \phi_w(x,y) + 2\pi k(x,y), \quad (5)$$

where $\Phi(x,y)$ is the unwrapped phase and $k(x,y)$ is an integer number called as fringe order.

2.2. Model of digital fringe projection system

In the DFP system, the well-known pinhole model is used to describe the imaging lens. Its mathematical expression can be written as

$$s^c[u^c, v^c, 1]^T = P^c[x^w, y^w, z^w, 1]^T, \quad (6)$$

$$P^c = A^c[R^c, t^c], \quad (7)$$

where s^c is a scale factor, superscript of c denotes camera, and superscript of w denotes the world coordinates.A^c is the intrinsic matrix of camera lens, and R^c and t^c are the extrinsic matrices. In this paper, we define P^c as the projection matrix of the camera lens. It can be used to describe the process of projecting 3D world coordinates (x^w, y^w, z^w) of object to 2D image coordinates (u^c, v^c). Since projecting images can be regarded as the inverse process of acquiring the images, the pinhole model can also be used to describe the imaging process of the projector [22].

$$s^p[u^p, v^p, 1]^T = P^p[x^w, y^w, z^w, 1]^T, \quad (8)$$

$$P^p = A^p[R^p, t^p], \quad (9)$$

where s^p is a scale factor and superscript of p denotes projector. A^p is the intrinsic matrix of projector lens, and R^p and t^p are the extrinsic matrices. P^p is the projection matrix of the projector lens used to describe the process of projecting 3D world coordinates (x^w, y^w, z^w) of object to 2D image coordinates (u^p, v^p).

2.3. The geometric constraint method

In this paper, the DFP system is calibrated using the method proposed in [22]. Then substituting the internal and external parameters of the system into the monotonic discriminant [14], we can determine the correct position of the virtual plane used in geometric constraint method for the constructed system. It is shown in this research that the depth of the object increases monotonically with the pixel coordinates of the projector, and therefore the closest distance, $z^w = z^w_{\min}$, is selected to be the position of the virtual plane.

Substituting $z^w = z^w_{\min}$ into equation (6), the correspondent $x^w_{\min}$ and $y^w_{\min}$ for each camera pixel (u^c, v^c) can be solved:

$$\begin{bmatrix} x^w_{\min} \\ y^w_{\min} \end{bmatrix} = \begin{bmatrix} p^c_{31}u^c - p^c_{11} & p^c_{32}u^c - p^c_{12} \\ p^c_{31}v^c - p^c_{21} & p^c_{32}v^c - p^c_{22} \end{bmatrix}^{-1} \begin{bmatrix} p^c_{14} - p^c_{34}u^c - (p^c_{33}u^c - p^c_{13})z^w_{\min} \\ p^c_{24} - p^c_{34}v^c - (p^c_{33}v^c - p^c_{23})z^w_{\min} \end{bmatrix}. \quad (10)$$

Then, with equation (8), the projector pixel coordinates of u^p can be solved:

$$u^p = \frac{p^p_{11}x^w_{\min} + p^p_{12}y^w_{\min} + p^p_{13}z^w_{\min} + p^p_{14}}{p^p_{31}x^w_{\min} + p^p_{32}y^w_{\min} + p^p_{33}z^w_{\min} + p^p_{34}}, \quad (11)$$

where p^c_{ij} and p^p_{ij} are the matrix elements of the P^c and P^p respectively, with subscripts of i and j being the row and column numbers respectively. In this research, we use fringe patterns along the vertical direction, because the vertical direction is close to the optimal fringe angle of the system [23]. After obtaining the projector pixel coordinates, we can get the absolute phase distribution on this virtual plane,

$$\Phi^V_{\min}(u^c, v^c) = \frac{2\pi}{T}u^p, \quad (12)$$

where T is the period of the fringe. Then, the fringe order can be determined which is as:

$$k(u^c, v^c) = ceil\left[\frac{\Phi^V_{\min}(u^c, v^c) - \phi_w(u^c, v^c)}{2\pi}\right]. \quad (13)$$

Substituting the determined fringe order into equation (5), the unwrapped phase of $\Phi_{absg}(u^c, v^c)$ is obtained which is an absolute phase distribution. The fundamental limitation of this method is the confined depth sensing range. The effective depth range can be expressed as

$$\Delta z = \frac{T_s}{\tan\alpha}, \quad (14)$$

where T_s is the fringe period of the projected pattern in space, and α is the angle between projector and camera optical axis. The detailed derivation process can be found in [12].

2.4. Windowed Fourier-filtering and quality-guided phase-unwrapping algorithm

2.4.1. Window Fourier-filtering method for fringe pattern analysis.

WFT has been widely used in optical metrology for fringe pattern analysis due to its robustness to noise. WFT and inverse WFT are pairs of transforms, and their mathematical expressions are written as

$$Sf(u,v,\xi,\eta) = \int_{-\infty}^{+\infty}\int_{-\infty}^{+\infty} f(x,y)g^*_{u,v,\xi,\eta}(x,y)\mathrm{d}x\mathrm{d}y = \mathrm{WFT}(f), \quad (15)$$

$$\begin{aligned} f(x,y) &= \frac{1}{4\pi^2}\int_{-\infty}^{+\infty}\int_{-\infty}^{+\infty}\int_{-\infty}^{+\infty}\int_{-\infty}^{+\infty} Sf(u,v,\xi,\eta) \\ &\quad g_{u,v,\xi,\eta}(x,y)dudvd\xi d\eta, \\ &= IWFT(Sf) \end{aligned} \quad (16)$$

where * denotes the complex conjugate operation, g is a window function which is selected as Gaussian function, and $f(x,y)$ is an exponential fringe pattern composed of wrapped phase obtained by three step phase shifting algorithm and can be expressed as:

$$f = \exp[j\phi_w(x,y)], \quad (17)$$

where $j = \sqrt{-1}$. In order to remove the noise in WFT spectrum, a threshold processing is taken: the spectrum is set to be zero if its amplitude is less than a preset threshold. The setting can be expressed as

$$\overline{Sf}(u,v,\xi,\eta) = \begin{cases} Sf(u,v,\xi,\eta) & if\ |Sf(u,v,\xi,\eta)| \geqslant thr \\ 0 & if\ |Sf(u,v,\xi,\eta)| < thr \end{cases}, \quad (18)$$

where $\overline{Sf}(u,v,\xi,\eta)$ denotes the spectrum distribution after thresholding and thr denotes the threshold value. The filtered fringe pattern can be written as

$$\bar{f}(x,y) = \mathrm{IWFT}(\overline{Sf}(u,v,\xi,\eta)). \quad (19)$$

The filtered fringe pattern is also an exponential function and can be rewritten as:

$$\bar{f}(x,y) = \bar{b}(x,y)\exp[j\overline{\varphi}_w(x,y)], \quad (20)$$

where $\bar{b}(x,y)$ denotes the filtered amplitude with its value reflecting the quality of the wrapped phase on each pixel, and $\overline{\varphi}_w(x,y)$ denotes the filtered wrapped phase.

2.4.2. Quality-guided phase-unwrapping algorithm.

The filtered amplitude of $\bar{b}(x,y)$ is selected as the quality map to guide the phase-unwrapping path of the filtered wrapped phase of $\overline{\varphi}_w(x,y)$. We adopt the classical guiding strategy [11] which is described as follows.

Step 1: Sort all the values of the quality map and select the pixel with the maximum value, such as that denoted by red 0 in figure 1, as the starting point of the phase unwrapping. Then

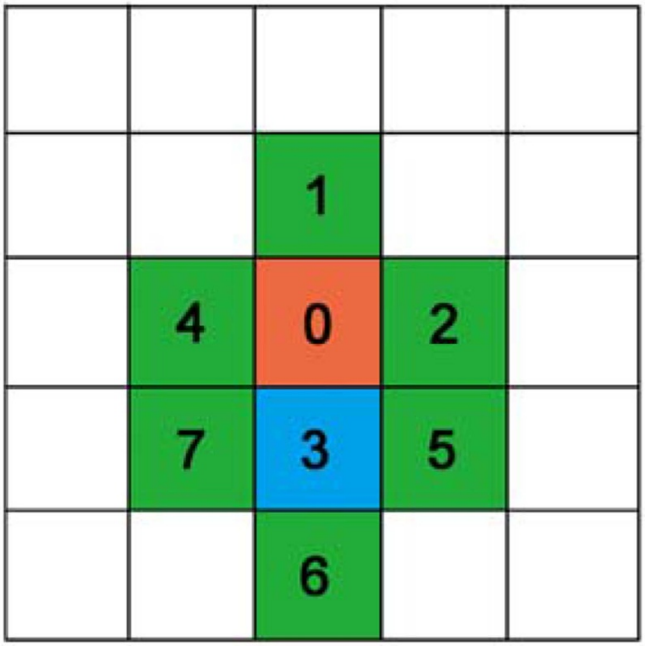

Figure 1. Diagram of QGPU process.

put its adjacent four phase points denoted by 1, 2, 3 and 4 in figure 1 into the adjoining list.

Step 2: Find the pixel with the maximum quality value from the adjoin list, denoted by blue 3 in figure 1, and unwrap the correspondent phase by referring to the phase value of the starting point. Then, remove it from the adjoin list and put its adjacent phase points that have not been processed, denoted by 5, 6 and 7 in figure 1, into the adjoin list.

Step 3: Select the pixel point with the maximum quality value in the adjoin list and unwrap the correspondent phase by referring to the last unwrapped phase value. Then remove it from the adjoin list and put its adjacent phase points that have not been processed into the adjoin list.

Step 4: Repeat step 3 until the adjoin list is empty.

It should be pointed out that there is still a limitation of π phase change between two successive points of the unwrapping path in the WFF-QGPU method.

2.5. Proposed depth extension method

The entire flowchart of the depth extension method proposed in this paper is shown in figure 2.

Step 1: The wrapped phase recovery. Firstly, the wrapped phase is obtained by the three-step phase shift method described in section 2.1. Then, the filtered wrapped phase is obtained by window Fourier-filtering method described in section 2.4.1.

Step 2: Absolute phase unwrapping. The filtered wrapped phase is unwrapped by geometric constraint method as described in section 2.3, and the unwrapped phase is denoted by Φ_{absg}. For the measurement of objects with large depth variances, there exist clearly dividing lines in the unwrapped phase map, which can be used for image segmentation.

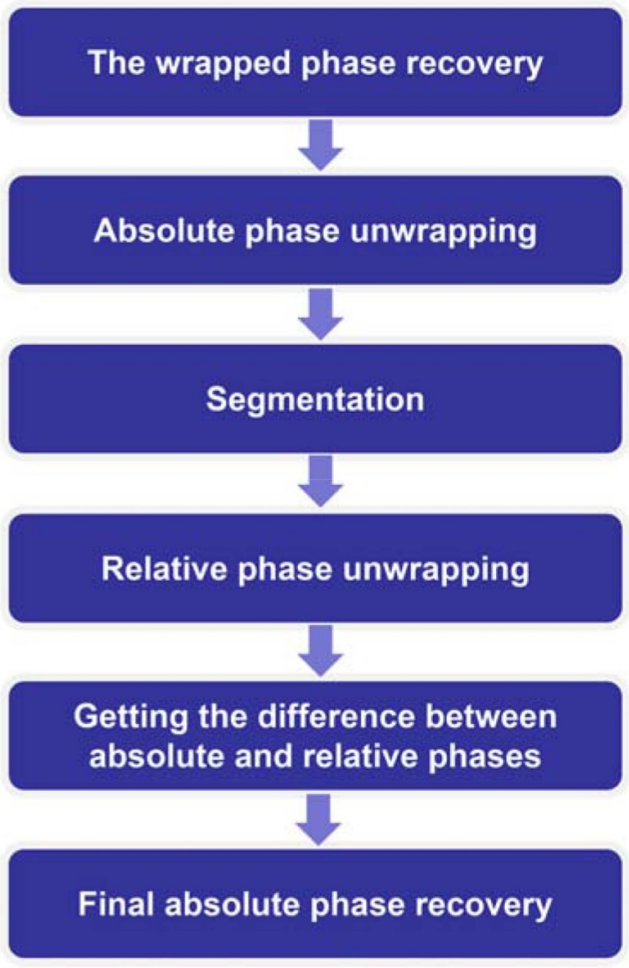

Figure 2. Flowchart of the proposed depth extension method.

Step 3: Segmentation. The pixel region with correct absolute phase values is extracted from the unwrapped phase in step 2, using the watershed image segmentation algorithm [24]. Then, a binary template, *mask*, is created for the extracted region.

Step 4: Relative phase unwrapping. The relative unwrapped phase of Φ_{rel} is acquired using WFF-QGPU method described in section 2.4. There is a relationship between the relative phase map and the absolute phase map, which can be expressed as:

$$\Phi_{abs} = \Phi_{rel} + \Delta\Phi, \tag{21}$$

where Φ_{abs} represents the absolute phase and $\Delta\Phi$ is a constant to be determined.

Step 5: Getting the difference between absolute and relative phases. $\Delta\Phi$ is determined by the unwrapped absolute phase acquired in step 2, the relative phase acquired in step 4 and the mask acquired in step 3. The process can be expressed as:

$$\Delta\Phi = \mathrm{Mode}((\Phi_{absg} - \Phi_{rel}) \times \mathrm{mask}), \tag{22}$$

where Mode() is function of taking the mode of a set of data.

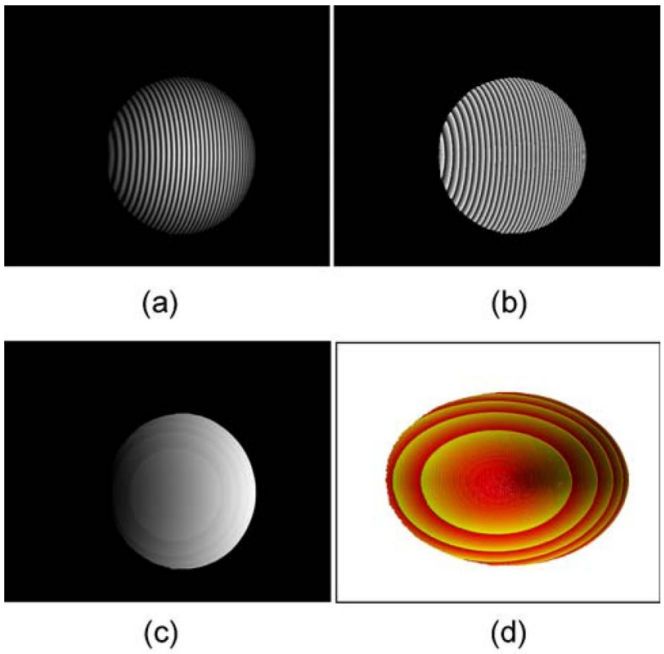

Figure 3. Measurement result of a single plaster ball using geometric constraint method. (a) One of the three-step phase shifting patterns; (b) the wrapped phase; (c) the unwrapped phase using geometric constraint method; (d) the 3D measurement result corresponding to (c).

Step 6: Final absolute phase recovery. Substituting the determined $\Delta\Phi$ into equation (21), the absolute phase map of the object is achieved.

3. Experiment

We construct a DFP system, including a single charge coupled device (CCD) camera (DAHENG MER-131-210U3M-L) and a single digital light processing (DLP) projector (DLP6500). The camera has a 12.5 mm focal length and the projector has a 23 mm focal length.

Firstly, we measure a smooth plaster ball for verifying the proposed method. Figure 3(a) is one of the three-step phase shifting fringe patterns acquired by the camera, where the fringe period of T is 21 pixels. Figure 3(b) shows the wrapped phase calculated by equation (4). Then, the unwrapped phase map is obtained using geometric constrain method which is shown in figure 3(c). Obviously, there exist clearly dividing lines in figure 3(c), indicating that the unwrapped phase map is discontinuous. Figure 3(d) is the 3D measurement result corresponding to figure 3(c), where the problem of limited measurement depth range of this unwrapping method can be found easily.

Then, we use the proposed method to extend the effective 3D measurement depth. An exponential fringe pattern expressed in equation (17) is generated and then the de-noised wrapped phase is obtained using WFF method (see step 1). Figure 4(a) shows the de-noised wrapped phase distribution. Figure 4(b) is the unwrapped phase distribution acquired by the geometric constraint method (see step 2). The watershed image segmentation algorithm is adopted to segment the image of figure 4(b) and the result is shown in figure 4(c) (see step 3). Based on prior knowledge, the center of the ball is closest to the virtual plane, and so the absolute phase values in the blue area of figure 4(c) are correct. Then, this region is identified and used to make a binary mask which is shown in figure 4(d). Figure 4(e) shows the relative phase distribution unwrapped by WFF-QGPU method and figure 4(f) is the unwrapping path map where the process is from light yellow pixel to dark red pixel successively (see step 4). The phase difference between figures 4(b) and (e) in the mask area, $\Delta\Phi$, is calculated which is 119.3805rad (see step 5). Then, by substituting the determined phase difference value into equation (21), the relative phase distribution is converted to absolute phase distribution (see step 6). Figure 4(g) shows the acquired absolute phase map where the phase distribution is continuous, and figure 4(h) gives the 3D measurement result of the plaster ball.

As a comparison, the same plaster ball is also measured by three-frequency phase-shifting method. The adopted three fringe periods are 21, 24 and 180 pixels, with three, five, and five phase shifting steps respectively. Figures 5(a)–(c) show the 3D measurement results obtained by the geometric constraint, the three-frequency phase-shifting and the proposed method, respectively. We present the depth distributions in these figures along a randomly selected row which are shown in figure 5(d). It can be seen that the depth distribution obtained by proposed method (red solid line) perfectly overlaps with that obtained by three-frequency phase-shifting method (blue dashed line). On the contrary, as the depth value of the object exceeds the sensing range, the geometric constraint method gives a wrong measurement result (green dot line).

To further evaluate the performance of the proposed method, a more complex object is measured, and figure 6(a) is the de-noised wrapped phase distribution acquired by WFF method (see step 1), where the fringe period of T is 34 pixels. Figure 6(b) is the unwrapped phase distribution acquired by the geometric constraint method (see step 2). There exist clearly dividing lines in figure 6(b), indicating that the unwrapped phase map is discontinuous. The watershed image segmentation algorithm is adopted to segment the image of figure 6(b), and the result is shown in figure 6(c) (see step 3). Based on prior knowledge, the yellow orange region in figure 6(c) is closest to the virtual plane, and so the absolute phase values in this region are correct. Then, this region is identified and used to make a binary mask which is shown in figure 6(d). Figure 6(e) shows the relative phase distribution unwrapped by WFF-QGPU method, and figure 6(f) is the unwrapping path map where the process is from light yellow pixel to dark red pixel successively (see step 4). The phase difference between figures 6(b) and (e) in the binary mask region, $\Delta\Phi$, is calculated which is 131.9469rad (see step 5). Then, by substituting the determined phase difference value into equation (21), the relative phase distribution is converted to the absolute phase distribution (see step 6). Figure 6(g) shows the acquired absolute phase map where the phase distribution is continuous. Figure 6(h) gives the 3D measurement result of the complex object.

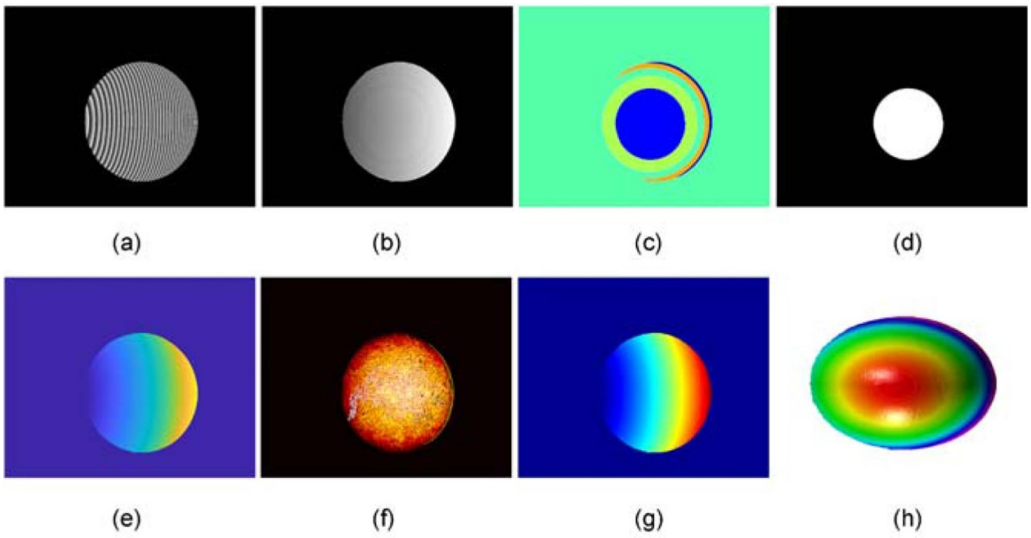

Figure 4. Measurement result of a single plaster ball using the proposed method. (a) The de-noised wrapped phase by WFF method; (b) the unwrapped phase by geometric constraint method; (c) segmenting result by watershed algorithm; (d) generated binary mask; (e) the relative phase map by WFF-QGPU; (f) the unwrapping path map; (g) the final absolute phase map; (h) 3D measurement result.

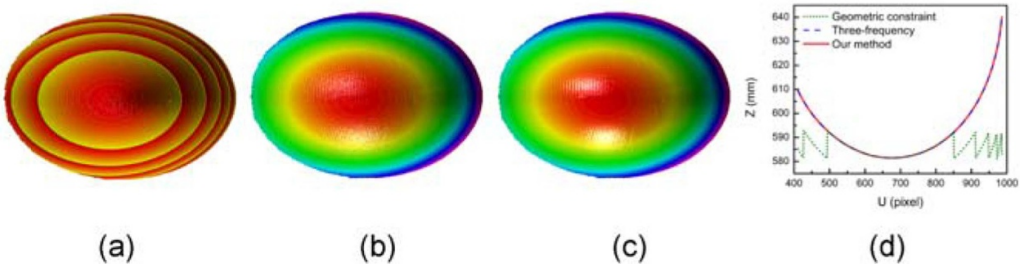

Figure 5. Comparison of the different methods. (a) 3D result acquired by the geometric constraint method; (b) 3D result acquired by three-frequency phase-shifting method; (c) 3D result acquired by the proposed method; (d) the depth distributions of (a)–(c) along a randomly selected row.

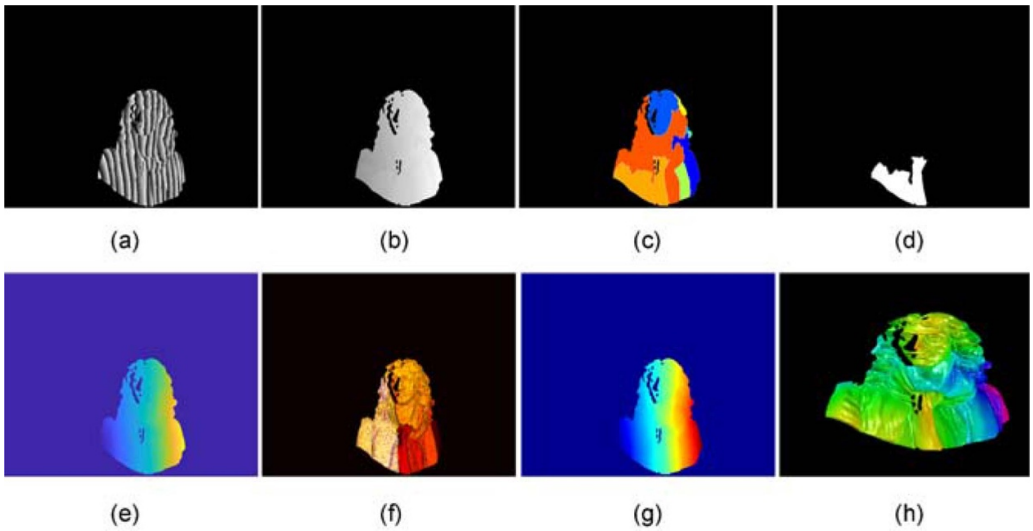

Figure 6. Measurement result of a complex object by the proposed method. (a) The de-noised wrapped phase by WFF method ($T = 34$ pixels); (b) the unwrapped phase by geometric constraint method; (c) image segmenting result using watershed algorithm; (d) generated binary mask; (e) the relative phase map by WFF-QGPU; (f) the unwrapping path map; (g) the final absolute phase map; (h) 3D measurement result.

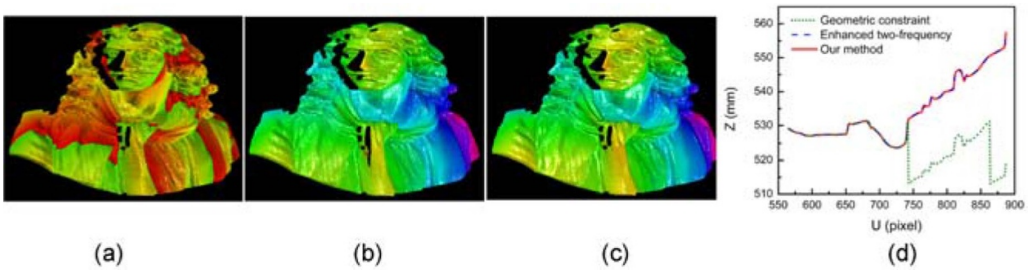

Figure 7. Comparison of different methods. (a) 3D measurement result acquired by the geometric constraint method; (b) 3D measurement result acquired by enhance two frequency phase-shifting method; (c) 3D measurement result acquired by the proposed method; (d) the depth distributions of (a)–(c) along a randomly selected row.

Figures 7(a)–(c) show the 3D measurement results obtained by the geometric constraint, the enhanced two-frequency phase-shifting [15] and the proposed method, respectively. For the enhanced two-frequency phase-shifting method, the fringe periods are set to be 30 and 126 pixels, with three and five phase-shifting steps, respectively. We present the depth distributions in these figures along a randomly selected row which are shown in figure 7(d). It can be seen that the depth distribution obtained by the proposed method (red solid line) perfectly overlaps with that obtained by enhanced two-frequency phase-shifting method (blue dash line). On the contrary, as the depth value of the object exceeds the sensing range, the geometric constraint method gives a wrong measurement result (green dot line).

4. Discussion

The proposed method of depth extension in 3D shape measurement by geometric constraints has the following merits and limitation.

4.1. Robustness to noise

WFT is a redundant transform, and its spectrum reflects the local characteristics of a signal. Thereby, the noise in the wrapped phase map can be well suppressed.

4.2. Simple region segmentation process

With the proposed method no additional virtual plane is required for the depth range extension in 3D shape measurement by geometric constraints, and so the region segmentation process is simple.

4.3. Limitation and solutions

WFF-QGPU is a type of SPU method and thus there exists limitation in the measurement of objects with abrupt geometric discontinuities. The object surface geometry, at least one unwrapping path, should not introduce more than π phase changes between two successive points. However, we found in our actual experiments that the limitation could be alleviated by changing the angle of the fringe pattern properly or by increasing the period of the fringe pattern appropriately.

5. Summary

We have demonstrated that the measurement depth limited by geometric constraints can be extended by the proposed method for the objects with large depth variances. Firstly, the correct part of the discontinuous absolute phase distribution acquired by geometric constraints is extracted, and the correspondent area is used to make a binary mask. Secondly, WFF-QGPU method, which has merit of suppressing noise, is adopted to realize relative phase unwrapping. Finally, the relative phase distribution is converted to the absolute phase distribution by referring to the acquired absolute phase values in the mask area. The effectiveness and correctness of the proposed method are verified by the actual 3D measurements of a plaster ball and a complex object in experiments.

Acknowledgments

This work is supported by The Scientific Instrument Developing Project of the Chinese Academy of Sciences, (YJKYYQ20180067), The Projects of Science Technology Development Plan of Jilin Province under Grant, (20190302102GX) and National Key Research and Development Project (2018YFC0308100 and 2018YFC0307900).

ORCID iD

Shenzhen Lv https://orcid.org/0000-0003-4112-5208

References

[1] Gorthi S and Rastogi P 2010 Fringe projection techniques: whither we are? *Opt. Laser Eng.* **48** 133–40
[2] Zhang S 2010 Recent progresses on real-time 3D shape measurement using digital fringe projection techniques *Opt. Laser Eng.* **48** 149–58
[3] Heist S, Dietrich P, Landmann M, Kuhmstedt P, Notni G and Tunnermann A 2018 GOBO projection for 3D measurements at highest frame rates: a performance analysis *Light Sci. Appl.* **7** 71
[4] Liu Y, Blunt L, Zhang Z, Rahman H A, Gao F and Jiang X 2020 In-situ areal inspection of powder bed for electron beam fusion system based on fringe projection profilometry *Addit. Manuf.* **31** 100940

[5] Takeda M and Mutoh K 1983 Fourier transform profilometry for the automatic measurement of 3-D object shapes *Appl. Opt.* **22** 3977
[6] Qian K 2004 Windowed Fourier transform for fringe pattern analysis *Appl. Opt.* **43** 2695–702
[7] Qian K 2007 Two-dimensional windowed Fourier transform for fringe pattern analysis: principles, applications and implementations *Opt. Laser Eng.* **45** 304–17
[8] Rivenson Y, Zhang Y, Gunaydin H, Teng D and Ozcan A 2018 Phase recovery and holographic image reconstruction using deep learning in neural networks *Light Sci. Appl.* **7** 17141
[9] Zhang S 2018 Absolute phase retrieval methods for digital fringe projection profilometry: a review *Opt. Laser Eng.* **107** 28–37
[10] Zuo C, Huang L, Zhang M, Chen Q and Asundi A 2016 Temporal phase unwrapping algorithms for fringe projection profilometry: a comparative review *Opt. Laser Eng.* **85** 84–103
[11] Su X and Chen W 2004 Reliability-guided phase unwrapping algorithm: a review *Opt. Laser Eng.* **42** 245–61
[12] An Y, Hyun J S and Zhang S 2016 Pixel-wise absolute phase unwrapping using geometric constraints of structured light system *Opt. Express* **24** 18445–59
[13] Liu X and Kofman J 2019 Real-time 3D surface-shape measurement using background-modulated modified Fourier transform profilometry with geometry-constraint *Opt. Laser Eng.* **115** 217–24
[14] Lv S, Sun Q, Zhang Y, Wang J and Jiang Y 2020 Monotonicity analysis of absolute phase unwrapping by geometric constraint in a structured light system *Opt. Express* **28** 9885–97
[15] Hyun J S and Zhang S 2016 Enhanced two-frequency phase-shifting method *Appl. Opt.* **55** 4395–401
[16] Li B, An Y and Zhang S 2016 Single-shot absolute 3D shape measurement with Fourier transform profilometry *Appl. Opt.* **55** 5219–25
[17] Li B, Liu Z and Zhang S 2016 Motion-induced error reduction by combining Fourier transform profilometry with phase-shifting profilometry *Opt. Express* **24** 23289–303
[18] Dai J, An Y and Zhang S 2017 Absolute three-dimensional shape measurement with a known object *Opt. Express* **25** 10384–96
[19] Duan M, Jin Y, Chen H, Kan Y, Zhu C and Chen E 2020 Dynamic 3-D shape measurement in an unlimited depth range based on adaptive pixel-by-pixel phase unwrapping *Opt. Express* **28** 14319–32
[20] Jiang C, Li B and Zhang S 2017 Pixel-by-pixel absolute phase retrieval using three phase-shifted fringe patterns without markers *Opt. Laser Eng.* **91** 232–41
[21] Qian K, Gao W and Wang H 2008 Windowed Fourier-filtered and quality-guided phase-unwrapping algorithm *Appl. Opt.* **47** 5420–8
[22] Zhang S and Huang P 2006 Novel method for structured light system calibration *Opt. Eng.* **45** 083601–08
[23] Wang Y and Zhang S 2013 Optimal fringe angle selection for digital fringe projection technique *Appl. Opt.* **52** 7094–8
[24] Vachier C and Meyer F 2005 The viscous watershed transform *J. Math. Imaging Vis.* **22** 251–67